JBC Papers in Press. Published on December 2, 2015 as Manuscript M115.705624
The latest version is at http://www.jbc.org/cgi/doi/10.1074/jbc.M115.705624

β-subunit binding is sufficient for ligands to open the integrin $\alpha_{IIb}\beta_3$ headpiece

Fu-Yang Lin[1], Jianghai Zhu[1], Edward T. Eng[1,2], Nathan E. Hudson[1], and Timothy A. Springer[1*]

[1]Department of Biological Chemistry and Molecular Pharmacology, Program in Cellular and Molecular Medicine, Boston Children's Hospital, Harvard Medical School, Boston, MA 02115, USA;
[2]Current address: New York Structural Biology Center, New York, NY
*Correspondence: timothy.springer@childrens.harvard.edu

Running Title: β-subunit binding and $\alpha_{IIb}\beta_3$ headpiece opening

Abstract

The platelet integrin $\alpha_{IIb}\beta_3$ binds to a KQAGDV motif at the fibrinogen γ-chain C-terminus and to RGD motifs present in loops in many extracellular matrix proteins. These ligands bind in a groove between the integrin α and β subunits; the basic Lys or Arg sidechain hydrogen bonds to the α_{IIb}-subunit and the acidic Asp sidechain coordinates to a metal ion held by the β_3-subunit. Ligand binding induces headpiece opening, with conformational change in the β-subunit. During this opening, RGD slides in the ligand-binding pocket towards α_{IIb}, with movement of the βI-domain β1-α1 loop toward α_{IIb}, enabling formation of direct, charged hydrogen bonds between the Arg sidechain and α_{IIb}. Here we test whether ligand interactions with β_3 suffice for stable ligand binding and headpiece opening. We find that the AGDV tetrapeptide from KQAGDV binds to the $\alpha_{IIb}\beta_3$ headpiece with affinity comparable to the RGDSP peptide from fibronectin. AGDV induced complete headpiece opening in solution as shown by increase in hydrodynamic radius. Soaking of AGDV into closed $\alpha_{IIb}\beta_3$ headpiece crystals induced intermediate states similarly to RGDSP. AGDV has very little contact with the α subunit. Furthermore, as measured by epitope exposure, AGDV, like the fibrinogen γ C-terminal peptide and RGD, caused integrin extension on the cell surface. Thus, pushing by the β_3 subunit on Asp is sufficient for headpiece opening and ligand sliding, and no pulling by the α_{IIb} subunit on Arg is required.

Introduction

Integrins are heterodimeric adhesion receptors that transmit outside-in as well as inside-out signals across the cell membrane. Ligands of αI-less integrins such as $\alpha_{IIb}\beta_3$ bind to a groove located in the interface between the α and β subunits (Fig 1) (1). When activated, the ectodomain of $\alpha_{IIb}\beta_3$ undergoes large-scale structural reshaping to an extended conformation with an open headpiece (Figure 1) and binds with high affinity to the two distal ends of a fibrinogen dimer, causing platelets to form tight aggregates (2,3). Arg-Gly-Asp (RGD) binding integrins, including $\alpha_{IIb}\beta_3$, $\alpha_v\beta_3$ and $\alpha_5\beta_1$, bind the Arg side chain to the β propeller domain of the α subunit via charged hydrogen bond(s). In contrast, the Asp sidechain of RGD coordinates to Mg^{2+} held in the metal ion-dependent adhesion site (MIDAS) and forms multiple hydrogen bonds to NH backbone amide groups, including two in the β1-α1 loop of the β subunit βI domain (3-5).

Within fibrinogen, $\alpha_{IIb}\beta_3$ binds not to RGD, but to a ^{400}HHLGGAKQAGDV^{411} sequence at the C-terminus of the γ subunit(3,6,7). Lys-406 of γC forms charged hydrogen bonds with the α_{IIb} subunit; that is, Lys-406 of γC is functionally equivalent to the Arg of RGD. The side chain carboxyl group of Asp-410 directly coordinates to the β_3 subunit MIDAS Mg^{2+} and forms hydrogen

bonds to the βI β1-α1 loop backbone, equivalently to the Asp of RGD (3). Additionally, the C-terminal α-carboxyl group of γC Val-411 forms a water-mediated, indirect coordination to the Ca^{2+} held in the adjacent to MIDAS (ADMIDAS) (3).

We recently soaked different concentrations of RGD peptide into crystals containing the $\alpha_{IIb}\beta_3$ headpiece in the closed conformation (assigned as state 1) and resolved six intermediate states (states 2-7) between the low-affinity closed headpiece and the high-affinity open headpiece (state 8) (4). Between states 1 and 8, the β1-α1 loop, which supplies three of the sidechains that coordinate the MIDAS Mg^{2+} ion, moved toward the Asp sidechain, enabling the Asp sidechain to form hydrogen bonds to β1-α1 loop backbone NH groups. RGD slid in its binding groove, enabling its Arg sidechain to closely approach α_{IIb} and to eventually form a charged hydrogen bond to α_{IIb} Asp-224. However, not until state 7 did a singular, well-resolved electron density map appear for the Arg sidechain. In states 1-6, the Arg side chain showed either weak density reflecting low occupancy, or multiple conformations, including water-mediated hydrogen bonds to Asp-224. In contrast, the Asp of RGD always had good density and always directly coordinated with the MIDAS Mg^{2+} ion, suggesting that Asp binding to the β subunit might be the main driver of headpiece opening. On the other hand, it was also possible that the attraction of the Arg sidechain to the oppositely charged Asp-224 in α_{IIb} was responsible for opening by pulling RGD, and with it the βI domain β1-α1 loop, toward α_{IIb}. Headpiece opening, rather than extension, is what greatly increases (by > 100-fold) integrin affinity for ligands (4,8). Headpiece opening is communicated across the βI domain by α_7-helix pistoning to swing-out of the hybrid domain (Fig. 1), which is a large-scale conformational change capable of being transmitted through the long integrin ectodomain legs to the cytoplasmic domains (1). Therefore, the question of whether headpiece opening is intrinsic to the β-subunit, or requires a pull by the α-subunit, is key to understanding both the biology and mechanochemistry of integrins.

To resolve this issue, we have examined binding to $\alpha_{IIb}\beta_3$ of truncated fibrinogen γC AGDV peptides that lack the Lys of KQAGDV, and thus cannot bind to the α_{IIb} subunit. Previous studies have shown that the QAGDV pentapeptide blocks binding of full-length fibrinogen to human platelets (9). Furthermore, CHO K1 cells transfected with $\alpha_{IIb}\beta_3$ could adhere to monolayers functionalized with AGD or RGD peptides equally well, and adhesion to AGDVC monolayers was inhibited by similar concentrations of RGDS and AGDV peptides (10). Our studies address multiple questions beyond the minimal requirements for integrin headpiece opening. These include how AGDV peptide can bind and activate, and the specific role of its C-terminal carboxyl group in interaction with the ADMIDAS.

Remarkably, we find comparable affinities of AGDV peptide, fibrinogen γC dodecapeptide, and RGD peptide for the $\alpha_{IIb}\beta_3$ integrin headpiece. AGDV can induce complete headpiece opening in solution, and crystals soaked with AGDV for varying durations defined the structural basis for AGDV-induced headpiece opening. Moreover, the C-terminal carboxyl of AGDV contributes to affinity by a highly geometrically constrained and hence highly specific water-mediated interaction with the ADMIDAS metal ion.

Experimental Procedures

Peptides. Fluorescein isothiocyanate–aminohexanoyl-HHLGGAKQAGDV (FITC-dodecapeptide) was synthesized by GenScript (Piscataway, NJ). Unlabeled fibrinogen γC dodecapeptide was from American Peptide Company (Sunnyvale, CA). All other peptides were synthesized by GenScript with >95% purity. Unless otherwise specified, peptides were not modified at either terminus.

Recombinant $\alpha_{IIb}\beta_3$ headpiece. Expression

and purification of $\alpha_{IIb}\beta_3$ headpiece was as described (11).

Fluorescence anisotropy binding assay. Binding affinities for different peptide ligands were measured using fluorescence anisotropy as described previously (12). Anisotropy is defined as $(F\| - F\perp)/(F\| + 2F\perp)$, where $F\|$ and $F\perp$ are the fluorescence intensities parallel and perpendicular to the excitation plane, respectively. mA units (shown in figures) correspond to 1,000 x anisotropy. FITC-dodecapeptide probe (3nM) affinity for the $\alpha_{IIb}\beta_3$ headpiece ($K_D^{F^*}$) was obtained by increasing the concentration of purified recombinant $\alpha_{IIb}\beta_3$ headpiece to saturation. $K_D^{F^*}$ was fitted using one-site, specific binding; i.e. $A = A_{max} * C_{itg}/(K_D^{F^*} + C_{itg})$, where A represents the anisotropy signal from specific binding, C_{itg} represents the concentration of integrin $\alpha_{IIb}\beta_3$ headpiece, and A_{max} is the maximum anisotropy signal. Background anisotropy obtained by adding an excess of 10 μM tirofiban was subtracted from anisotropy.

After determining $K_D^{F^*}$, unlabeled peptides were used to compete FITC-dodecapeptide probe (3 nM) binding to 300 nM $\alpha_{IIb}\beta_3$ headpiece. I_{50} values for unlabeled peptides were obtained by least squares fitting. I_{50} values were converted to affinity values (K_D^p) for each peptide of interest using (12):

$$K_D^p = \frac{[F^*\alpha]_{50} \cdot IC_{50} \cdot K_D^{F^*}}{({F^*}_T \cdot \alpha_T) + [F^*\alpha]_{50} \cdot (\alpha_T - {F^*}_T + [F^*\alpha]_{50} - K_D^{F^*})}$$

where $K_D^{F^*}$ is the FITC-dodecapeptide binding affinity to $\alpha_{IIb}\beta_3$ headpiece (643 nM), ${F^*}_T$ is the total concentration of FITC-dodecapeptide (3 nM), α_T is the total concentration of $\alpha_{IIb}\beta_3$ headpiece (300 nM), IC_{50} and I_{50} are the free and total concentrations of the peptide of interest causing the displacement of 50% of specifically bound FITC-dodecapeptide (i.e., $IC_{50} = I_{50} - 0.5*300nM$), and $[F^*\alpha]_{50}$ is the concentration of FITC-dodecapeptide bound to $\alpha_{IIb}\beta_3$ headpiece at I_{50}. All measurements were in 20 mM HEPES pH 7.5, 150 mM NaCl, 1 mM $MnCl_2$, 0.2 mM $CaCl_2$. Prism GraphPad (La Jolla ,CA) program was used to fit the saturation binding curve, inhibition curves, and I_{50} values.

Size-exclusion chromatography and dynamic light scattering (DLS). The $\alpha_{IIb}\beta_3$ headpiece with coiled-coils was treated with chymotrypsin (chymotrypsin/integrin mass ratio = 1/200) at room temperature (13) for ~16 hours to remove C-terminal α-helical coiled-coils and to leave intact the thigh domain in the α subunit. Digested headpiece was purified by passage through a Ni-NTA column (13). For Stokes radius measurements, the re-purified headpiece at 10 μM (1 mg/ml by A_{280}) was incubated with 1 mM peptide ligand in 20 mM Tris-buffered saline (TBS) with 1 mM Mg^{2+} and 1 mM Ca^{2+} at 25°C for 30 minutes, and then applied to a Superdex 200 column (GE Healthcare Life Sciences) pre-equilibrated with the same buffer containing 1 mM peptide. Calibration and conversion of elution volume to Stokes radius was as described (11). For DLS, 20 μM chymotrypsin-treated, re-purified headpiece was filtered through a 100 nm cutoff membrane (Millipore Ultrafree Centrifugal Filter), incubated with 1 mM peptide in TBS plus 1 mM Mg^{2+}/Ca^{2+} for 10 minutes at 25°C in the cuvette, and read in the Viscotek 802 DLS (Viscotek Corporation). The DLS derived hydration radii (R_h) were obtained by intensity-based fitting using the OmniSize program for 2 to 3 independent measurements using the same batch of integrin headpiece sample, but measured in different days. Each measurement was an average of at least fifteen 10-second reads.

Crystallization, ligand soaking, and structure determination. The $\alpha_{IIb}\beta_3$ headpiece was crystallized in the closed conformation with the thigh domain removed (11). Briefly, chymotrypsin and carboxypeptidase-treated $\alpha_{IIb}\beta_3$/10E5 Fab complex was concentrated to 10

mg/mL in TBS (20 mM Tris, 150 mM NaCl, pH 7.4) with 1 mM Mg^{2+}, 1 mM Ca^{2+} and crystallized in 11% PEG 8000, 0.2M ammonium sulfate, 0.1M Tris-HCl, pH 8.9 at 4°C (11). Crystals were then stabilized with the same crystallization buffer but containing 15% PEG 8000, and glycerol concentration was incremented in 5% steps to 20% for cryoprotection. Finally, crystals were soaked in peptide in the same buffer with defined metal conditions for a specified duration at 4°C (Table 1). Diffraction data were collected at beamline ID-23 of Advanced Photon Source (Argonne, IL). Resolution limit was determined by cross-correlation (14). Refinements using Phenix (15) were as described (4).

Ligand-induced binding site (LIBS) epitope expression. CHO K1 cells stably transfected with full-length $\alpha_{IIb}\beta_3$ (16) were incubated at room temperature with serially-diluted peptide in 20 mM HEPES, pH 7.4, 150 mM NaCl, 5.5 mM glucose, 1% BSA, 1 mM Mg^{2+}/Ca^{2+}, and 10 μg/ml of LIBS1 antibody for 30 minutes. Mixtures were washed twice in the same buffer minus LIBS1. The washed cells were incubated with FITC-conjugated anti-mouse antibody at room temperature for 30 minutes, washed again, chilled on ice and subjected to flow cytometry. The dose-response curves were fit and EC_{50} values were calculated by Prism GraphPad.

Results

Affinities of peptides lacking Arg or Lys for the $\alpha_{IIb}\beta_3$ headpiece.

Truncated fibrinogen γC peptides such as QAGDV and AGD have been shown to block fibrinogen binding to platelets with similar IC_{50} values of ~100 μM (9), but more precise affinity measurements are required in order to understand the contribution of Lys or Arg. To test whether the Arg of RGD or Lys of KQAGDV is required for integrin binding, we quantitated the binding affinity to 300 nM purified $\alpha_{IIb}\beta_3$ headpiece in buffer with 2 mM Mn^{2+} and 0.1 mM Ca^{2+} using fluorescence polarization anisotropy. The fluorescent probe FITC-aminohexanoyl-HHLGGAKQAGDV bound saturably with a dissociation constant (K_D) = 0.64 ± 0.13 μM (Fig. 2A). Competition with fluorescent probe at 3 nM and integrin at 300 nM was then used to determine the K_D values of different peptides (Fig. 2B-F) (Materials and Methods). The fibrinogen γC dodecapeptide and fibronectin hexapeptide GRGDSP showed K_D of 1.27 ± 0.08 and 0.41 ± 0.26 μM, respectively (Figure 1B, C). In contrast, QAGDV and AGDV bound more weakly, with K_d of 7.85 ± 2.53 and 9.03 ± 2.75 μM, respectively (Figure 1D, E). N-acetylated AGDV (Ac-AGDV) binds ~9 times more strongly (K_d = 1.00 ± 0.46 μM, Figure 1F) than unmodified AGDV. Thus, Ac-AGDV has an affinity almost identical to the native γC dodecapeptide (Fig. 2B-F).

AGDV induces complete headpiece opening in solution.

We determined whether headpiece opening can occur without the Arg of RGD or the Lys of fibrinogen γC peptide. AGDV-induced opening (*i.e.*, hybrid domain swing-out, Figure 1B and C) of a six-domain $\alpha_{IIb}\beta_3$ headpiece fragment was measured as an increase in Stokes radius (Fig. 3) (11). The hydrodynamic radii of closed and open six-domain $\alpha_{IIb}\beta_3$ conformations were estimated from crystal structures (3,17) with HYDROPRO (18) as 4.68 nm and 5.03 nm, respectively. When incubated with 1 mM dodecapeptide and RGDF peptide (a high-affinity ligand of $\alpha_{IIb}\beta_3$,(19)), in the resting condition (TBS pH 7.4 plus 1mM Mg^{2+} and Ca^{2+}), the Stokes radius of $\alpha_{IIb}\beta_3$ headpiece increased from 4.69 ± 0.02 nm to 5.22 ± 0.06 nm and 5.19 ± 0.04 nm, respectively (Figure 3A) as measured by dynamic light scattering (DLS). A similar increase (to 5.24 nm ± 0.03) was observed with 1 mM AGDV peptide. The change in Stokes radius was also measured by size-exclusion chromatography (Fig. 3B). The elution volume shifted from 12.56 ± 0.01 in buffer

alone to 12.15 ± 0.06 ml in the presence of 1mM RGDF and to 12.19 ± 0.05 ml in AGDV. The corresponding Stokes radius shifted from 4.78 nm in buffer to 5.23 nm in RGDF and to 5.17 nm in AGDV (Fig. 3A). The DLS and gel-filtration results (Fig. 3A) demonstrated that a Lys or Arg residue is not essential for inducing full headpiece opening in $\alpha_{IIb}\beta_3$, since at 1 mM peptide concentration, AGDV, dodecapeptide, and RGD caused virtually indistinguishable increases in Stokes radius.

Crystal structures.

We soaked AGDV peptide into $\alpha_{IIb}\beta_3$ headpiece crystals in the closed conformation (state 1) in 1 mM Mn^{2+} and 0.2 mM Ca^{2+} and were able to trap four distinct intermediate states during headpiece opening (Table 1). Soaking times varied from 2 h to 1 week; the $t_{1/2}$ value for diffusion of a ligand of comparable size (fluorescein) into crystals of size comparable to ours (0.2 mm x 0.05 mm x 0.01 mm) is 16 min (20). Two copies of the $\alpha_{IIb}\beta_3$ headpiece complex (molecules 1 and 2) exist in one asymmetric unit (4), so we were able to obtain two different conformational states in a single crystal (Table 1). Based on the conformation and position of the moving parts of the βI domain, i.e., the β1-α1 loop, α1 helix, β6-α7 loop, and the ADMIDAS metal, each intermediate (Fig. 4) is assigned a state number between 1 (Fig. 4A) and 8 (Fig. 4B) corresponding to previous RGD-bound intermediates (4). AGDV binds in the groove formed between the α and β subunits (Fig. 4C, E, G, I), but has limited contact with α, because it occupies only a portion (about two-thirds) of the groove occupied by RGD (Fig. 4B). The N-terminal amine of AGDV is > 9.0 Å away from Asp-224 of α_{IIb}, which forms salt bridges to the Arg of RGD and the Lys of KQAGDV. Moreover, unlike the extended backbone conformation adopted by RGD (Fig. 4A, B), the backbone of AGDV is curved (Fig. 4C, E, G, I).

Compared to RGD (Fig. 4A, B) and dodecapeptide structures in complex with the natively open headpiece in state 8 (Fig. 4J), the Φ angle of Gly of AGDV is rotated about 180º (Fig. 4C, E, G, I). This correlates with the markedly different backbone carbonyl oxygen orientation of the Arg in RGD (Fig. 4A, B, F) and Ala in KQAGDV (Fig. 4J) compared to Ala in AGDV and AGDV-NH_2 (Fig. 4C-E and G-I). The peptide α-amino group, with a pKa estimated to be around 8, is weakly basic, and would be partially charged at the binding assay pH of 7.4 and the crystallization pH of 8.9. To test for a weak π-cation interaction between the N-terminal primary amine and Tyr-190 of α_{IIb} (plan distance ~4 Å), we abolished protonation by N-terminal acetylation. Acetylation increased peptide affinity (Fig. 2F) and therefore ruled out a contribution by a charged α–amino group to AGDV to binding.

Overall, the intermediate states caused by AGDV are similar to those induced by GRGDSPK (4) (Fig. 4). The exception is AGDV state 3, in which the β1-α1 loop backbone is shifted similarly to that with RGD in state 3, but the ADMIDAS Ca^{2+} ion is shifted more towards the MIDAS and has lost its coordinations to Asp-126 and Asp127 (Fig. 4E). In contrast, the ADMIDAS Ca^{2+} ion retained its Asp-126 and Asp-127 coordinations in RGD state 3 (Fig. 4F). However, electron density for the ADMIDAS Ca^{2+} in AGDV state 3 is weak, which suggests an ill-defined position in shape-shifting. Importantly, during soaking for one week, AGDV induced the β_3 subunit in molecule 1 in crystals to shift to state 7, i.e., almost all the way to the open conformation, despite little interaction with the α_{IIb} subunit (Fig. 4I).

The pathway of AGDV-induced headpiece opening.

The Asp carboxylate of AGDV in state 2 (Fig. 4C) shows a different angle from later states (Fig. 4E, G, I), with one carboxyl oxygen coordinating the MIDAS, and the other oxygen pointing away from the binding pocket. In this orientation, the ligand Asp would clash with Tyr-122 side chain in the following states. In state 3, the Asp carboxyl re-orientates to enable for Tyr-122 and Ser-123 in the β1-α1 loop to move closer to the

ligand, and forms a hydrogen bond with the Tyr-122 backbone (Fig. 4E). Between states 2 and 3, the side chain hydroxyl of Ser-123 moves closer to ligand and replaces a water molecule in the MIDAS to directly coordinate with the MIDAS metal ion (Fig. 4C to 4E). The direct coordination of the Ser-123 sidechain to the MIDAS and the hydrogen bond between the Asp of AGDV and the Tyr-122 backbone each remain in place through later states. However, also between states 2 and 3, the valine side chain of AGDV switches to a different rotamer that is sustained through state 7 and the C-terminal carboxyl group rotates toward the ADMIDAS metal (Fig. 4E, G and I compared to 4C).

In state 6, the β1-α1 loop continues its movement toward ligand (Fig. 4G). At this point, the Cβ carbon of Ser-123 is 2.4 Å away from its position in state 1. In state 6, the ADMIDAS metal ion is 3.4 Å away from its position in state 1, and is much closer to the C-terminal carboxyl of AGDV (4.8 Å). Importantly, starting from state 6, the C-terminal carboxyl of AGDV forms an indirect, water-mediated coordination with the ADMIDAS metal ion (Fig. 4G). Between states 6 and 7, the Cα atoms of Asp-126 and Asp-127 on the α1 helix move 2.2 Å toward the ADMIDAS metal ion (and 3.5 Å from state 1) and form direct coordinations (Fig. 4I). In addition, the β6-α7 loop flips away from the ADMIDAS to accommodate movement of the α1 helix toward ligand (Fig. 4G and I). In state 7, the conformations of the β1-α1 loop, α1 helix, and ADMIDAS metal of βI are very close to the natively open state 8 bound to fibrinogen γC dodecapeptide (Fig. 4I compared to 4J). The α–carboxyl of AGDV now forms a stronger 2.7 Å hydrogen bond with an ADMIDAS-coordinating water molecule (Fig. 4I).

The C-terminal carboxyl group is not required for headpiece opening.

We tested the role of the AGDV peptide α-carboxyl group in headpiece opening. We first measured the affinities of a series of C-terminally modified AGDV peptides, including AGDV-NH_2 (amidated), AGDV-OCH_3 (O-methylated), and AGD(v) (D-valine in place of L-valine). Both AGDV-NH_2 and AGDV-OCH_3 showed weaker binding than AGDV, with 5.6-fold and 7.5-fold reductions in affinity, respectively (Fig. 2G, H), in agreement with results using amidated dodecapeptide (21). On the other hand, substituting L-valine with D-valine in AGD(v) resulted in a more pronounced, 24-fold decrease in binding affinity (Fig. 2I). These results clearly demonstrate that the contact between the α-carboxyl moiety of γC and the ADMIDAS metal ion makes an important contribution to affinity and is highly specific both for the carboxyl group and the chirality of the Val residue.

A free C-terminus was not required for headpiece conformational change. At 1 mM (20 x K_D), amidated-AGDV increased the hydrodynamic radius from 4.69 nm to 5.04 nm, while at 1 mM (100 x K_D), AGDV increased the radius to 5.2 nm (Fig. 3A). Attempts to increase the concentration of AGDV-NH_2 to 2.5 and 5 mM resulted in headpiece aggregation. However, the use of AGDV at 140 μM (16 x K_D) and 480 μM (50 x K_D) induced similar shifts in Stokes radius as AGDV-NH_2 at 1 mM (20 x K_D) (Fig. 3A), showing that when corrected for amount of binding, AGDV-NH_2 and AGDV are similar in ability to induce headpiece opening.

When closed headpiece crystals were soaked with 50 mM AGDV-NH_2 for 2 h, the peptide was observed in both integrin molecules in the asymmetric unit, with molecule 1 in state 5 (Fig. 4H) and molecule 2 in state 3 (Fig. 4D). Similar soaking for 2 h with AGDV resulted in binding to headpiece molecule 1 in state 6 and molecule 2 in state 3 (Fig. 4G and E). The slightly less shape-shifting induced by AGDV-NH_2 is compatible with its lower affinity. The conformation of AGDV-NH_2 in state 5 is similar to AGDV in states 6 and 7. The main difference is that the terminal amide oxygen of AGDV-NH_2 is 3.9 Å away from the ADMIDAS water (Fig. 4H), while the corresponding distance in AGDV states 6 and 7 are 3.0 and 2.7 Å, respectively (Fig. 4G, I). The conformations of Val of AGDV-NH_2 and AGDV

in states 5-8 are very similar (Fig. G-J). In state 3, the ADMIDAS metal ion position with AGDV-NH_2 (Fig. 4D) resembled that with RGD (Fig. 4F) rather than with AGDV (Fig. 4E).

A dicarboxylate $\alpha_{IIb}\beta_3$ antagonist.

Some $\alpha_{IIb}\beta_3$ antagonists have two carboxyl groups, such as Ro-435054 (22) (Fig. 7A). To test whether the second carboxyl group would orient similarly to the α–carboxyl group of KQAGDV and AGDV, we soaked Ro-435054 into crystals. However, crystals were preserved when we soaked with 1 mM Ro-435054 for 2 h in Mg^{2+}/Ca^{2+}. The compound bound to both $\alpha_{IIb}\beta_3$ molecules in the asymmetric unit and induced shape shifting to states 6 and 3 (Table 1). This contrasts with soaking for 24 h with 10 mM GRGDSP in Mg^{2+}/Ca^{2+}, which only shifted molecule 1 to state 2 and bound to molecule 2 without shifting it from state 1 (4). Density for Ro-435054 was well-defined; however, electron densities for ADMIDAS Ca^{2+} ions in both molecules were very weak, and ADMIDAS Ca^{2+} ions were therefore omitted during refinement. Ro-435054 is a peptidomimetic. One of the nitrogens in its N-terminal benzamidine overlaps with the ε-amino group of the Lys side chain of KQAGDV. Most importantly, the sidechain carboxyl of the Asp residue and the α-carboxyl groups of the Phe residue of Ro-435054 align very well with those of the Asp and Val residues of γC dodecapeptide and AGDV (Fig. 7B).

AGDV induces integrin extension on cell surfaces similarly to RGD peptide and fibrinogen dodecapeptide.

Exposure of ligand-induced binding site (LIBS) epitopes on integrin $\alpha_{IIb}\beta_3$ is widely used as a surrogate of conformational change; however, the type of conformational change (e.g. integrin extension or headpiece opening) that LIBS antibodies report on $\alpha_{IIb}\beta_3$ is poorly characterized. Detergent soluble, intact $\alpha_{IIb}\beta_3$ particles purified from human platelets are 91% in the bent conformation (23). Incubation with LIBS1 Fab fragment had little effect on the proportion of bent particles (95%) and no binding of LIBS1 Fab was detected by EM (Fig. 5A). After incubation with the high affinity RGD-mimetic L-739758 (24) at a final concentration of 10 nM, plus 1 mM Mn^{2+} and 0.1 mM Ca^{2+}, most particles are in extended conformations (23); LIBS1 bound to the lower β-leg of extended $\alpha_{IIb}\beta_3$, near the EGF4 and β-tail domains (Fig. 5B and C). These results show that LIBS1 exposure does not occur in bent $\alpha_{IIb}\beta_3$ and requires extension; since the RGD-mimetic also induces headpiece opening, it remains to be determined whether LIBS1 binding requires headpiece opening in addition to extension.

GRGDSP, γC dodecapeptide, and AGDV dose-dependently elicited LIBS1 binding to CHO cells stably expressing full-length human $\alpha_{IIb}\beta_3$ (Fig. 6). AGDV induces the same maximal LIBS1 epitope exposure (extension) as GRGDSP and dodecapeptide in 1 mM Mg^{2+} and 1 mM Ca^{2+}. However, potencies differ; AGDV is 2.5 times less effective compared to dodecapeptide (EC_{50} of 1.43 mM vs. 0.58 mM), and ~7 times less effective than GRGDSP (EC_{50} = 0.21 mM).

Discussion

We have shown that the AGDV peptide can bind to $\alpha_{IIb}\beta_3$ integrin with affinity comparable to GRGDSP peptide and fibrinogen γC dodecapeptide, and is capable of inducing complete integrin headpiece opening in solution. The structural basis for AGDV-induced headpiece opening was determined by soaking AGDV into crystals and observing a series of intermediate conformational states. AGDV peptides differing in C-terminal modifications showed that the indirect coordination between the α-carboxyl of AGDV and the ADMIDAS metal ion contributes to affinity for $\alpha_{IIb}\beta_3$. Binding of AGDV peptide is also able to induce LIBS1 epitope exposure and hence full-length $\alpha_{IIb}\beta_3$ integrin extension on cell surfaces.

Crystal structures showed that AGDV has limited contact with the α_{IIb} subunit. Of the total

solvent-accessible surface area (SASA) (25) buried by AGDV on $\alpha_{IIb}\beta_3$ (~340 Å^2), only 23% (80 Å^2) is contributed by the α_{IIb} subunit. The α_{IIb} subunit contributes no specific interactions. In contrast, the tetrapeptide has a much larger, 260-Å^2 interface with β, or 77% of the total buried SASA. Relative to typical interfaces buried in antibody-protein antigen interactions of 800 Å^2 (26), the overall burial of AGDV is small. Thus the highly specific contacts made by AGDV must be important. The interface between AGDV and the integrin βI domain includes multiple hydrogen bonds with the β1-α1 loop, and most importantly, the coordination of Asp side chain carboxyl to the MIDAS metal, and the water-mediated contact with the ADMIDAS metal.

Unlike RGD or γC dodecapeptide, AGDV peptides do not form salt bridges with the integrin α_{IIb} subunit. Despite lacking the salt bridges, Ac-AGDV shows an almost identical affinity with dodecapeptide, and AGDV peptide is only ~7 times less potent than the dodecapeptide in Mn^{2+}/Ca^{2+}. These observations show that the contribution in binding free energy of the salt bridge and other additional contacts with α are relatively minor compared to the interactions with β.

The C-terminal carboxyl group of AGDV contributes positively to binding based on the ~7-fold reduction in affinity with amidated AGDV (AGDV-NH_2). Nevertheless, the α-carboxyl group is not required for headpiece opening. In DSL experiments, similar saturation of the headpiece with AGDV-NH_2 and AGDV gave similar increases in hydrodynamic radius. Moreover, AGDV and AGDV-NH_2 induced similar headpiece opening when soaked into crystals.

In aggregate, our results show that Asp binding to the β_3 subunit contributes the majority of the energy for ligand binding, and that interaction with the β_3 subunit is sufficient to induce headpiece opening and extension. These findings also suggest that β_3 integrins may have broader ligand specificities than previously expected.

The native C-terminal carboxyl of AGDV peptide was more favorable than any other chemical modification we tested, including amidation, methylation, and replacing the C-terminal L-valine with a D-valine. The order of affinity was native carboxyl > amide > methyl ester > D-valine). The C-terminal carboxyl group forms a water mediated coordination to the ADMIDAS metal (Fig. 4G, I) (3). One explanation for the weaker affinity of AGDV-NH_2 is that the long-range ionic interaction (4.7 Å) between the α-carboxyl anion and ADMIDAS divalent metal cation is absent in AGDV-NH_2. The other explanation is the different hydrogen bond strength among these derivatives. A charged carboxyl oxygen forms a stronger hydrogen bond to water than an uncharged carbonyl oxygen in an amide or ester. Interestingly, the chirality of Val of AGDV was very important, since substitution with D-valine resulted in a 24-fold reduction in affinity. These results are consistent with the identical orientation and rotamer of the Val sidechain in AGDV and AGDV-NH_2 states 3-7 and in native state 8 of the dodecapetide. The α-carboxyl group of D-valine cannot form polar contacts with the ADMIDAS, since the side chain of D-valine will clash with Tyr-122 of the β_3 subunit when its α-carboxyl group is oriented identically to that of L-valine.

The di-carboxylate $\alpha_{IIb}\beta_3$ antagonist Ro-435054 binds the high affinity state of $\alpha_{IIb}\beta_3$ ~100-fold better (K_D= 6 nM) than the low affinity state (K_D= 580 nM) (27). Ro-435054 is a 4-residue peptidomimetic, with an N-terminal amidinobenzoyl, β-alanine, L-Asp, and C-terminal L-Phe (Fig. 7A). Most interestingly, the C-terminal Phe residue of Ro-435054 adopts an identical orientation to the Val of KQAGDV and AGDV and thus may be considered a fibrinogen-mimetic. The high affinity RGDF peptide (19) may be considered both fibrinogen and RGD-mimetic. RGDF has the same two C-terminal amino acids as R0-435054, and may be predicted to bind similarly.

Following fibrin formation in hemostasis, fibrin molecules are cross-linked by factor XIIIa. Factor XIIIa catalyzes the transglutamination

reaction between Lys-406 of γC in one fibrin molecule and Gln-398 or Gln-399 in another to crosslink two neighboring dimers (28). Gln-399 immediately precedes the γC dodecapeptide and in the dodecapeptide, Lys-406 is the Lys of KQAGDV that binds to α_{IIb}. This C-terminal portion of the fibrinogen γC-subunit is unstructured in absence of binding to $\alpha_{IIb}\beta_3$. While factor XIIIa covalently stabilizes fibrin, it at the same time makes Lys-406 unavailable for integrin binding. Since our results demonstrate that this Lys is not required for binding to $\alpha_{IIb}\beta_3$, it is conceivable that the cross-linked fibrin may still interact with $\alpha_{IIb}\beta_3$ using the C-terminal AGDV sequence. Further investigations on $\alpha_{IIb}\beta_3$ binding to factor XIIIa-crosslinked fibrin are needed to understand the physiological relationship between fibrin crosslinking and binding to $\alpha_{IIb}\beta_3$.

Acknowledgement

Supported by NIH grant HL103526. We thank the GM/CA beamline of the Advanced Photon Source (APS). GM/CA@ APS has been funded in whole or in part with Federal funds from the National Cancer Institute (Y1-CO-1020) and the National Institute of General Medical Science (Y1-GM-1104). Use of the Advanced Photon Source was supported by the U.S. Department of Energy, Basic Energy Sciences, Office of Science, under contract No. W-31-109-ENG-38. We thank Dr. Paul B. Gillespie from Roche for providing Ro-435054. We also thank Drs. Xianchi Dong and Adem Koksal for collecting part of the X-ray diffraction data, and finally Dr. Jieqing Zhu for helpful discussions.

Author Contribution

F.-Y.L., J.Z., E.T.E contributed to research design, carried out experiments, analyzed data and wrote the manuscript. N.E.H. analyzed the data and helped prepare the manuscript. T.A.S. conceived the experimental design, analyzed the data and wrote the manuscript.

Conflict of Interests

None.

References

1. Springer, T. A., and Dustin, M. L. (2012) Integrin inside-out signaling and the immunological synapse. *Curr. Opin. Cell Biol.* **24**, 107-115
2. Weisel, J. W., Nagaswami, C., Vilaire, G., and Bennett, J. S. (1992) Examination of the platelet membrane glycoprotein IIb-IIIa complex and its interaction with fibrinogen and other ligands by electron microscopy. *J. Biol. Chem.* **267**, 16637-16643
3. Springer, T. A., Zhu, J., and Xiao, T. (2008) Structural basis for distinctive recognition of fibrinogen by the platelet integrin $\alpha_{IIb}\beta_3$. *J. Cell Biol.* **182**, 791-800
4. Zhu, J., Zhu, J., and Springer, T. A. (2013) Complete integrin headpiece opening in eight steps. *J. Cell Biol.* **201**, 1053-1068
5. Xiong, J. P., Stehle, T., Zhang, R., Joachimiak, A., Frech, M., Goodman, S. L., and Arnaout, M. A. (2002) Crystal structure of the extracellular segment of integrin $\alpha_V\beta_3$ in complex with an Arg-Gly-Asp ligand. *Science* **296**, 151-155
6. Farrell, D. H., Thiagarajan, P., Chung, D. W., and Davie, E. W. (1992) Role of fibrinogen α and γ chain sites in platelet aggregation. *Proc. Natl. Acad. Sci. U S A* **89**, 10729-10732
7. Holmback, K., Danton, M. J., Suh, T. T., Daugherty, C. C., and Degen, J. L. (1996) Impaired platelet aggregation and

sustained bleeding in mice lacking the fibrinogen motif bound by integrin αIIbβ3. *EMBO J.* **15**, 5760-5771

8. Schürpf, T., and Springer, T. A. (2011) Regulation of integrin affinity on cell surfaces. *EMBO J.* **30**, 4712-4727
9. Kloczewiak, M., Timmons, S., Lukas, T. J., and Hawiger, J. (1984) Platelet receptor recognition site on human fibrinogen synthesis and structure-function relationship of peptides corresponding to the carboxy-terminal segment of the gamma chain. *Biochemistry* **23**, 1767-1774
10. Sanchez-Cortes, J., and Mrksich, M. (2009) The platelet integrin αIIbβ3 binds to the RGD and AGD motifs in fibrinogen. *Chem. Biol.* **16**, 990-1000
11. Zhu, J., Negri, A., Provasi, D., Filizola, M., Coller, B. S., and Springer, T. A. (2010) The closed headpiece of integrin $\alpha_{IIb}\beta_3$ and its complex with an $\alpha_{IIb}\beta_3$-specific antagonist that does not induce opening. *Blood* **116**, 5050-5059
12. Rossi, A. M., and Taylor, C. W. (2011) Analysis of protein-ligand interactions by fluorescence polarization. *Nat. Protoc.* **6**, 365-387
13. Xiao, T., Takagi, J., Wang, J.-H., Coller, B. S., and Springer, T. A. (2004) Structural basis for allostery in integrins and binding of fibrinogen-mimetic therapeutics. *Nature* **432**, 59-67
14. Karplus, P. A., and Diederichs, K. (2012) Linking crystallographic model and data quality. *Science* **336**, 1030-1033
15. Adams, P. D., Afonine, P. V., Bunkoczi, G., Chen, V. B., Davis, I. W., Echols, N., Headd, J. J., Hung, L. W., Kapral, G. J., Grosse-Kunstleve, R. W., McCoy, A. J., Moriarty, N. W., Oeffner, R., Read, R. J., Richardson, D. C., Richardson, J. S., Terwilliger, T. C., and Zwart, P. H. (2010) PHENIX: a comprehensive Python-based system for macromolecular structure solution. *Acta Crystallogr. D Biol. Crystallogr.* **66**, 213-221
16. Luo, B.-H., Springer, T. A., and Takagi, J. (2003) Stabilizing the open conformation of the integrin headpiece with a glycan wedge increases affinity for ligand. *Proc. Natl. Acad. Sci. U. S. A.* **100**, 2403-2408
17. Zhu, J., Luo, B. H., Xiao, T., Zhang, C., Nishida, N., and Springer, T. A. (2008) Structure of a complete integrin ectodomain in a physiologic resting state and activation and deactivation by applied forces. *Mol. Cell* **32**, 849-861
18. Garcia De La Torre, J., Huertas, M. L., and Carrasco, B. (2000) Calculation of hydrodynamic properties of globular proteins from their atomic-level structure. *Biophys. J.* **78**, 719-730
19. Andrieux, A., Hudry-Clergeon, G., Ryckewaert, J. J., Chapel, A., Ginsberg, M. H., Plow, E. F., and Marguerie, G. (1989) Amino acid sequences in fibrinogen mediating its interaction with its platelet receptor, GPIIbIIIa. *J. Biol. Chem.* **264**, 9258-9265
20. Geremia, S., Campagnolo, M., Demitri, N., and Johnson, L. N. (2006) Simulation of diffusion time of small molecules in protein crystals. *Structure* **14**, 393-400
21. Kloczewiak, M., Timmons, S., Bednarek, M. A., Sakon, M., and Hawiger, J. (1989) Platelet receptor recognition domain on the γ chain of human fibrinogen and its synthetic peptide analogues. *Biochemistry* **28**, 2915-2919
22. Alig, L., Edenhofer, A., Hadvary, P., Hurzeler, M., Knopp, D., Muller, M., Steiner, B., Trzeciak, A., and Weller, T. (1992) Low molecular weight, non-peptide fibrinogen receptor antagonists. *J. Med. Chem.* **35**, 4393-4407
23. Eng, E., Smagghe, B., Walz, T., and Springer, T. A. (2011) Intact $\alpha_{IIb}\beta_3$ extends after activation measured by solution X-ray scattering and electron microscopy. *J. Biol. Chem.* **286**, 35218-35226
24. Egbertson, M. S., Cook, J. J., Bednar, B., Prugh, J. D., Bednar, R. A., Gaul, S. L.,

Gould, R. J., Hartman, G. D., Homnick, C. F., Holahan, M. A., Libby, L. A., Lynch, J. J., Jr., Lynch, R. J., Sitko, G. R., Stranieri, M. T., and Vassallo, L. M. (1999) Non-peptide GPIIb/IIIa inhibitors. 20. Centrally constrained thienothiophene alpha-sulfonamides are potent, long acting in vivo inhibitors of platelet aggregation. *J. Med. Chem.* **42**, 2409-2421

25. Krissinel, E., and Henrick, K. (2007) Inference of macromolecular assemblies from crystalline state. *J. Mol. Biol.* **372**, 774-797

26. Janin, J. (1997) Specific versus non-specific contacts in protein crystals. *Nature Struc.Biol.* **4**, 973-974

27. Bednar, R. A., Gaul, S. L., Hamill, T. G., Egbertson, M. S., Shafer, J. A., Hartman, G. D., Gould, R. J., and Bednar, B. (1998) Identification of low molecular weight GP IIb/IIIa antagonists that bind preferentially to activated platelets. *J. Pharmacol. Exp. Ther.* **285**, 1317-1326

28. Strong, D. D., Moore, M., Cottrell, B. A., Bohonus, V. L., Pontes, M., Evans, B., Riley, M., and Doolittle, R. F. (1985) Lamprey fibrinogen γ chain: cloning, cDNA sequencing, and general characterization. *Biochemistry* **24**, 92-101

Figure Legends

Figure 1. Integrin domains and conformational changes. Integrins are heterodimers of α and β subunits, each with large N-terminal extracellular domains, transmembrane domains (TM), and usually short C- terminal cytoplasmic domains. αIIbβ3 can adopt three major conformations: (A) bent with closed headpiece, (B) extended with closed headpiece, and (C) extended with open headpiece (17,23). Colored dashed lines emphasize the flexibility of the lower β-leg and lack of correlation of its position, in absence of applied force, with whether the headpiece is open or closed. In integrin headpiece opening, downward pistoning of the α7-helix (black bar) of the βI domain is linked to swing-out of the hybrid domain (curved arrow) and rearrangement of loops at the ligand-binding site. The open headpiece (C) has high affinity to ligands.

Figure 2. Saturation binding, competition curves, and calculated K_d values from fluorescence anisotropy. (A) Saturation binding of FITC-dodecapeptide. (B-I) Competitive binding of the indicated peptides. The K_d values were calculated from IC_{50} values as described in Experimental Procedures.

Figure 3. Peptide ligands without Arg or Lys can induce full headpiece opening in Mg^{2+}/Ca^{2}. (A) Stokes radii measured by dynamic light scattering (DLS, triplicate, mean and s.d.) and size exclusion chromatography (Superdex 200, duplicate, mean and difference from mean). nd = not determined. (B) Overlaid Superdex 200 chromatograms of unclasped αIIbβ3 headpiece in absence (green), or presence of 1mM RGDF peptide (purple), or 1mM AGDV peptide (blue).

Figure 4. Crystal structures. Structures with soaked in AGDV and AGDV-NH_2 determined here (C-E and G-I) are compared to previously determined structures (A-B, F, and J) (3,4). Residues of the α_{IIb} and β_3 subunits are shown with wheat and cyan carbons, respectively. MIDAS and ADMIDAS metals are shown as grey and yellow spheres, respectively. Smaller red spheres represent water molecules. Black dashes represent hydrogen bonds and metal ion coordinations.

Figure 5. Electron microscopy (EM) class-averages of full-length $\alpha_{IIb}\beta_3$. $\alpha_{IIb}\beta_3$ purified from platelets in buffer with dodecylmaltoside (23) was mixed with LIBS1 Fab and subjected to gel filtration and negative stain EM, particle picking, and class averaging as described (23). (A) Representative class averages of $\alpha_{IIb}\beta_3$ and LIBS1 Fab mixture, showing LIBS1 does not bind to $\alpha_{IIb}\beta_3$ in the closed-bent conformation in 1 mM Mg^{2+} plus 1 mM Ca^{2+}. (B) Representative EM class averages of $\alpha_{IIb}\beta_3$ bound to fragment of

LIBS1 Fab in the presence of 10 nM L-739,759 and 1 mM Mn^{2+} plus 0.1 mM Ca^{2+}. (C) Schematic diagram of integrin domains and approximate binding regions of LIBS1 antibody as shown by EM. (D) All 30 EM class averages from (B); each box has a dimension of 120x120 pixels with 4.5 Å/pixel. The number of particles in each class average is denoted in each box.

Figure 6. Peptide ligands induce integrin extension on cell surface. $\alpha_{IIb}\beta_3$ transfectants in presence of indicated peptides were stained with LIBS1 antibody, stained with FITC anti-IgG, and subjected to flow cytometry. MFI= mean fluorescence intensity.

Figure 7. Structure of Ro-435054 bound to $\alpha_{IIb}\beta 3$ headpiece. (A) Chemical structure of Ro-435054; (B) overlay of $\alpha_{IIb}\beta_3$ complex crystal structures with Ro-435054 (green carbons) and γC dodecapeptide (grey carbons), after superimposition on main chain atoms of the βI domain. Only $\alpha_{IIb}\beta_3$ residues from the Ro-435054 complex are illustrated with carbons colored wheat (α_{IIb}) or cyan (β_3). The MIDAS Mg^{2+} is shown as a grey sphere, and water molecules as small red spheres. Black dashed lines represent hydrogen bonds and metal coordinations of the Ro-435054 structure.

Table 1. X-ray diffraction and structure refinement statistics.

Ligand	50 mM AGDV (Mn/Ca), 1 week	50 mM AGDV (Mn/Ca), 2 hrs	50 mM AGDV-NH_2 (Mn/Ca), 2 hrs	1 mM Ro-435054 (Mg/Ca), 2 hrs
Data collection[a]				
Space group	$P2_12_12$	$P2_12_12$	$P2_12_12$	$P2_12_12$
Unit cell (a, b, c) (Å)	256.9, 144.4, 104.6	259.9, 144.5, 104.7	259.4, 144.3, 104.6	259.3, 144.4, 105.0
(α, β, γ) (°)	90, 90, 90	90, 90, 90	90, 90, 90	90, 90, 90
Resolution (Å)	50-2.60 (2.64-2.60)	50-2.85 (2.90-2.85)	50-2.75 (2.80-2.75)	50-2.70 (2.77-2.70)
Completeness (%)	97.5 (73.9)	99.6 (94.0)	94.9 (87.9)	98.6 (87.0)
R_{merge}	22.2 (427)	18.9 (362)	15.1 (208)	17.1 (243)
I/σ(I)	12.7 (0.4)	18.2 (0.3)	10.2 (0.6)	4.84 (0.4)
$CC_{1/2}$	99.4 (18.6)	98.5 (12.9)	98.7 (18.9)	98.4 (10.8)
Refinement[a]				
Resolution (Å)	50-2.60 (2.64-2.60)	50-2.85 (2.90-2.85)	50-2.75 (2.80-2.75)	50-2.70 (2.77-2.70)
No. of reflections	117,195 (5,179)	92,354 (5,041)	107,747 (10,641)	106,571 (9,580)
R_{work}	0.230 (0.385)	0.227 (0.395)	0.188 (0.320)	0.213 (0.361)
R_{free}	0.252 (0.425)	0.252 (0.414)	0.236 (0.334)	0.234 (0.365)
CC_{work}	0.946 (0.466)	0.926 (0.258)	0.939 (0.377)	0.950 (0.363)
CC_{free}	0.907 (0.229)	0.911 (0.384)	0.890 (0.595)	0.954 (0.521)
No. non-hydrogen atoms				
Protein	20771	20791	20878	20835
Ligand / ion	50 / 14	50 / 14	50 / 14	78 / 12
Water	670	585	992	674
B factors				
Protein	96.5	117	97.3	92.6
Ligand / ion	72.0 / 101	101 / 134	78.0 / 116	71.6 / 89.33
Water	59.7	64.2	60.4	59.8
r.m.s. deviations				
Bond lengths (Å)	0.003	0.005	0.004	0.002
Bond angles (°)	0.680	0.640	0.662	0.630
molecules/ asym. unit	2	2	2	2
Conformational states (molecule 1/molecule 2)	State 7/State 2	State 6/State 3	State 5/State 3	State 6/State 3
PDB code	4Z7N	4Z7O	4Z7Q	4Z7S

[a] Numbers in the parentheses correspond to the highest resolution shell.
Mn/Ca: 2 mM $MnCl_2$, 0.1 mM $CaCl_2$
Mg/Ca: 1 mM $MgCl_2$, 1 mM $CaCl_2$

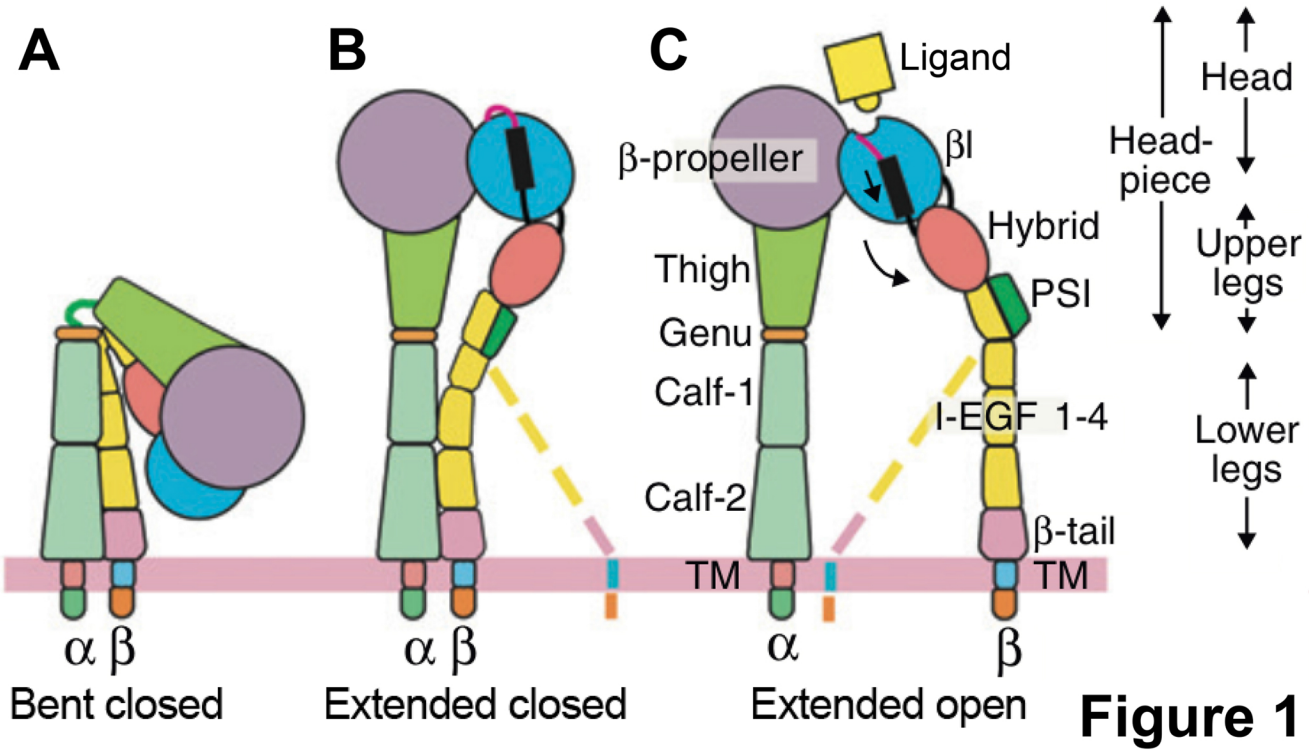

Figure 1

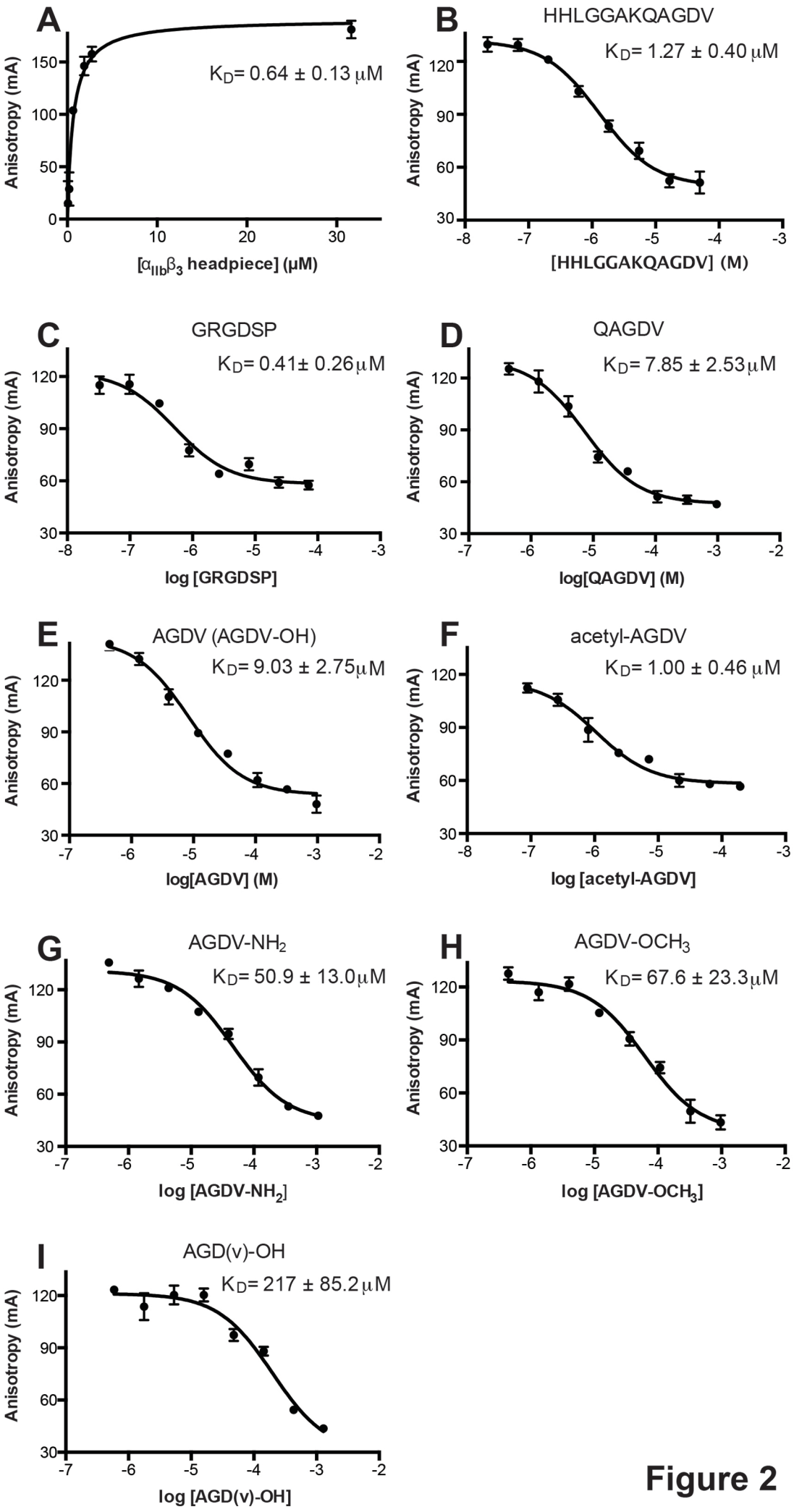

Figure 2

Figure 3

A Stokes radii by dynamic light scattering (DLS) and size exclusion column

	DLS (nm)	Size-exclusion (nm)
$\alpha_{IIb}\beta_3$ headpiece alone	4.69 ± 0.02	4.78 ± 0.02
$\alpha_{IIb}\beta_3$ + 1 mM γC dodecapeptide	5.22 ± 0.06	nd
$\alpha_{IIb}\beta_3$ + 1 mM RGDF-OH (RGDF)	5.19 ± 0.04	5.23 ± 0.07
$\alpha_{IIb}\beta_3$ + 1 mM AGDV-OH (AGDV)	5.24 ± 0.03	5.17 ± 0.06
$\alpha_{IIb}\beta_3$ + 0.14 mM AGDV-OH	4.96 ± 0.03	nd
$\alpha_{IIb}\beta_3$ + 0.48 mM AGDV-OH	5.00 ± 0.06	nd
$\alpha_{IIb}\beta_3$ + 1 mM AGDV-NH_2	5.04 ± 0.06	nd

B

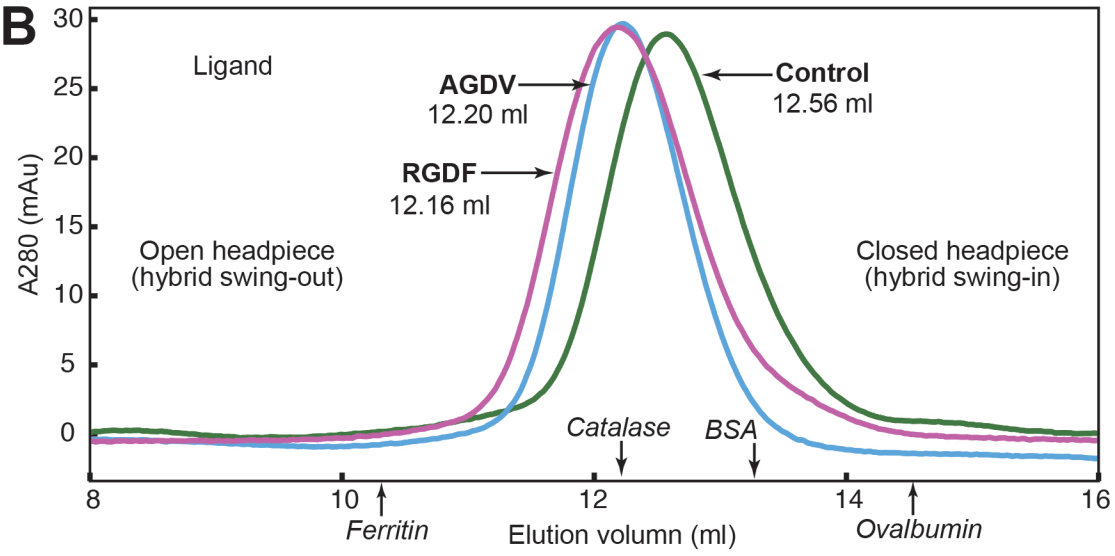

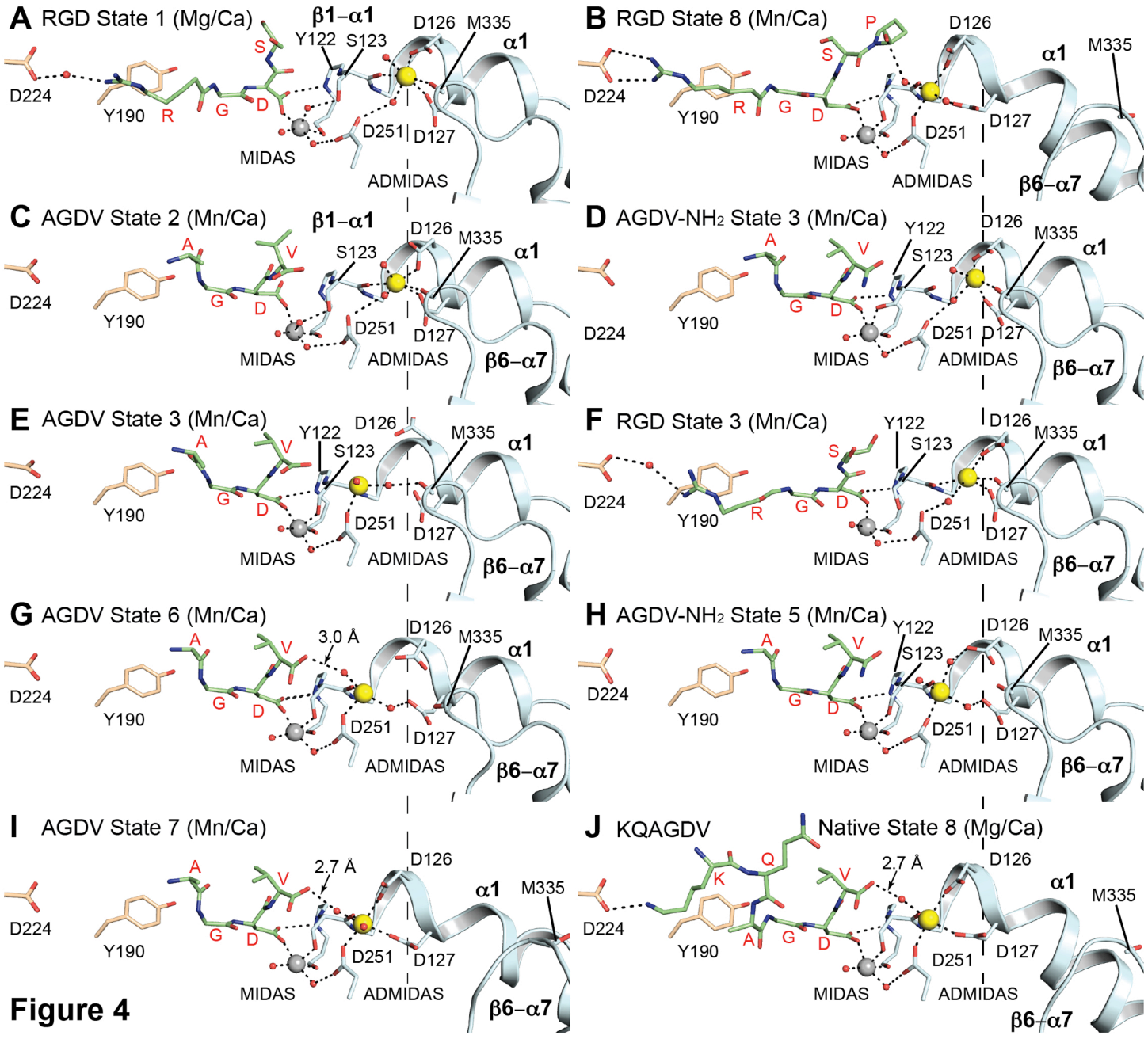

Figure 4

Figure 5

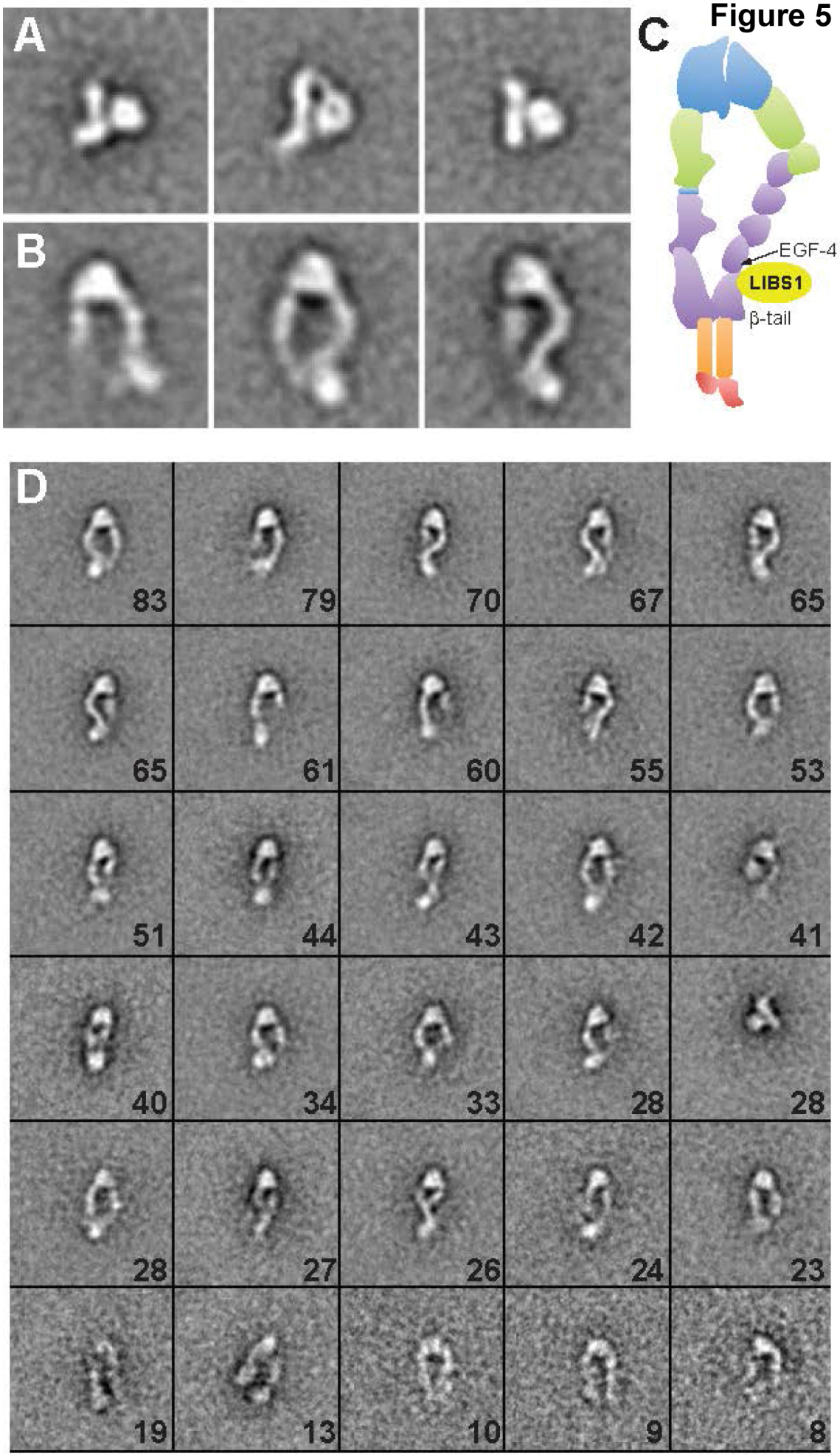

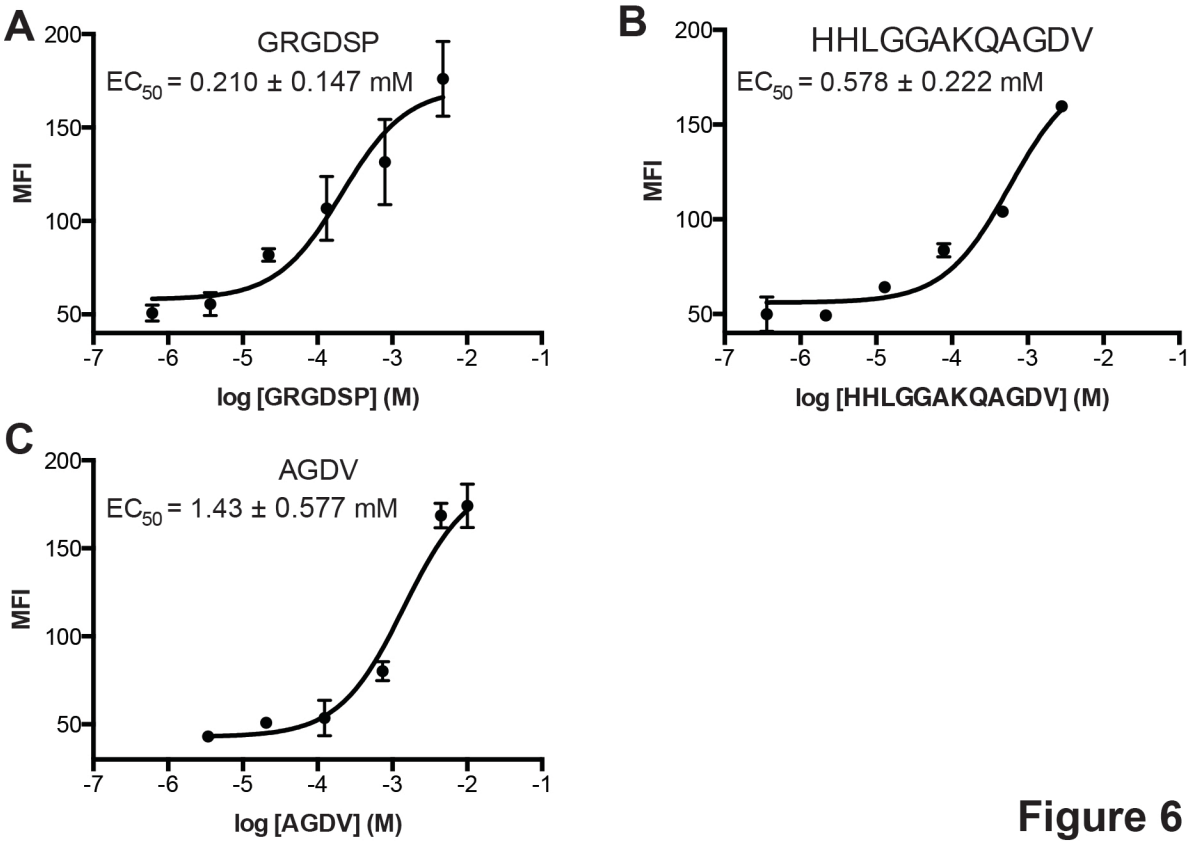

Figure 6

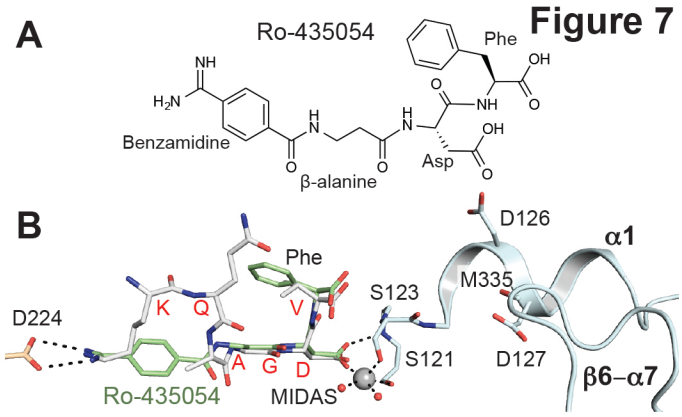

Figure 7

β-subunit Binding is Sufficient for Ligands to open the Integrin αIIbβ3 Headpiece

Fu-Yang Lin, Jianghai Zhu, Edward T. Eng, Nathan E. Hudson and Timothy A. Springer

J. Biol. Chem. published online December 2, 2015
